Forward Electron Compton Scattering and Absolute Energy Calibration of the Tagged Photon Beam in Hall B

(Letter of Intent)

May 28, 2002

L. Gan
University of North Carolina at Wilmington, Wilmington, NC

A. Gasparian, A. Ahmidouch, S. Danagoulian
North Carolina A&T State University, Greensboro, NC

D. Dale
University of Kentucky, Lexington, KY

D. Lawrence, R. Miskimen
University of Massachusetts, Amherst, MA

M. Khandaker, C. Salgado
Norfolk State University, Norfolk, VA

A. Margaryan
Yerevan Physics Institute, Yerevan, Armenia

D. Sober
The Catholic University of America, Washington, DC

A. Afanasev, M. Ito, V. Kubarovsky
Thomas Jefferson National Accelerator Facility, Newport News, VA

A.M. Bernstein
Massachusetts Institute of Technology, Cambridge, MA

E. Pasyuk, B.G. Ritchie
Arizona State University, Tempe, AZ

P.L. Cole
University of Texas at El Paso, El Paso, TX

R. Minehart
University of Virginia, Charlottesville, VA

A. Glamazdin
Kharkov Institute of Physics and Technology, Kharkov, Ukraine

V.P. Likhachev
Instituto de Fsica da Universidade de Sao Paulo, Sao Paulo, SP, Brasil

Abstract

We propose to determine the absolute energy of the tagged photon beam in Hall B from 2.0–5.7 GeV with a precision of 0.1–0.2% via electron Compton scattering near the minimum opening angle of the photon-electron system. The same data will also allow us to extract the differential cross sections of Compton scattering in the forward angles at the $\sim 2\%$ level. This will be a first precise measurement on this interaction process in the few GeV energy range, and will shed light on the higher order corrections to the Klein-Nishina formula. The proposed measurement will use the PrimEx experimental setup, including a state-of-the art high resolution hybrid electro-magnetic calorimeter (HYCAL).

Contents

1 Introduction

The scattering of photons by free electrons is one of the simplest and most basic quantum-electrodynamic processes that is experimentally accessible. Since A.H. Compton first presented a semi-quantum mechanical treatment of such an interaction in 1922 [1], many theoretical calculations of the characteristics of Compton scattering have been developed. Compton scattering in the few GeV energy region provides an important tool for measuring the photon beam energy with high precision ($\sim$ 0.1–0.2% level). In addition, it also reveals a valuable piece of information about the radiative corrections [2]-[4] to the Compton cross section which have not been tested experimentally.

1.1 Motivation

1.1.1 Absolute Energy Measurement of the Tagged Photon Beam

For high precision photo-production experiments, having the energy of the photon beam very well defined plays a crucial role in the overall accuracy of the measurement. One such example is E99-014 (PrimEx) in Hall B, an A-rated experiment under preparation to perform a high precision (1.4%) measurement of the $\pi^0 \to \gamma\gamma$ decay width. The experiment will measure the π^0 lifetime via small angle coherent photo-production of the π^0 in the Coulomb field of a nucleus, *i.e.*, via the Primakoff effect.

For unpolarized photons, the Primakoff cross section is given by [5]:

$$\frac{d^3\sigma_P}{d\Omega} = \Gamma_{\gamma\gamma}\frac{8\alpha Z^2}{m^3}\frac{\beta^3 E^4}{Q^4}|F_{e.m.}(Q)|^2 sin^2\theta_\pi \qquad (1)$$

where $\Gamma_{\gamma\gamma}$ is the π^0 decay width, Z is the atomic number, m, β, θ_π are the mass, velocity and production angle of the pion, E is the energy of the incoming photon, Q is the momentum transfer to the nucleus, and $F_{e.m.}(Q)$ is the nuclear electro-magnetic form factor, corrected for final state interactions of the outgoing pion.

The peak value of the Primakoff cross section has a strong energy dependence, proportional to E^4, and hence it is very critical to have a precise knowledge of the absolute energy of the photon beam. The photon tagging facility in Hall B, to be used for the PrimEx experiment, will provide a big advantage over previous Primakoff experiments, in both photon energy and flux control. Currently, the absolute energy determination of this facility is known at the $\sim$ 1% level. Developing an independent method to determine the absolute energy of the tagged photon beam is critical. Electron Compton scattering can provide a unique way to measure the absolute value of the energy of the tagged photon beam with an accuracy of $\sim$ 0.1%.

1.1.2 Test of Higher-Order Corrections to the Klein-Nishina Formula

Electron Compton scattering is one of the simplest and most fundamental reactions in QED. The lowest order Compton scattering diagrams (see figure 1) were first calculated by Klein and Nishina in 1929 [7], and by Tamma in 1930 [8]. There are two types of corrections to the basic Klein-Nishina formula which must be considered when studying Compton scattering at energies above 0.1 GeV. These are radiative corrections, and double Compton scattering contributions where one of the final state photons is soft. Figure 2 shows Feynman diagrams illustrating these two processes. The interference between the basic first-order single Compton scattering amplitude and the radiative and double Compton scattering amplitudes have been studied extensively in the literature [2]-[4], [9]-[10]. Figure 3 shows the percentage corrections to the Klein-Nishina total cross section from these contributions. These studies suggest that the higher order corrections to the first-order Klein-Nishina formula would be about 5–10% [11] when the beam energy is ≥ 1 GeV.

However, experiments done so far are mostly in the energy region below 0.1 GeV and a few in the range 0.1–1.0 GeV with an accuracy of 10 to 15% [12]-[15]. Only one experiment [11] measured the Compton scattering total cross section up to 5.0 GeV using a bubble-chamber detection method and the measurement errors for energies above 1 GeV were at the 20–70% level. Due to the lack of precision experimental data, higher order corrections to the Klein-Nishina formula have never been tested experimentally. With the PrimEx setup we can measure the Compton scattering cross section in the 2.0–5.7 GeV region in the forward angles with an accuracy of $\sim 2\%$ which will fill this important experimental gap. The proposed experimental measurements projected to the Klein-Nishina differential cross section are shown in figure 4.

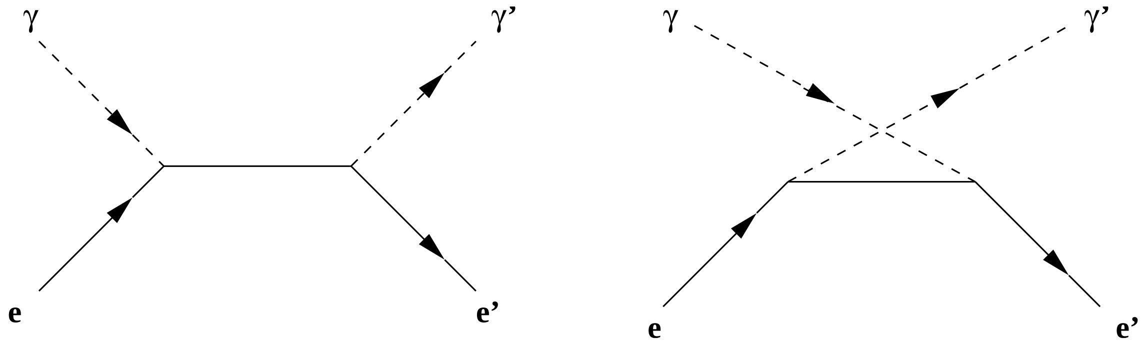

Figure 1: The lowest-order Feynman diagrams for single Compton scattering.

(a) (b)

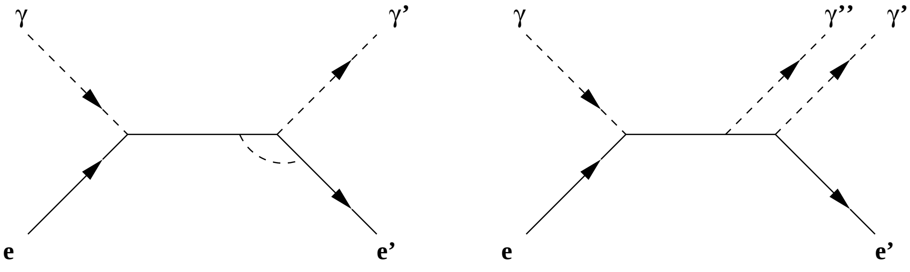

Figure 2: Typical (a) radiative correction, and (b) double Compton scattering contributions to single Compton scattering.

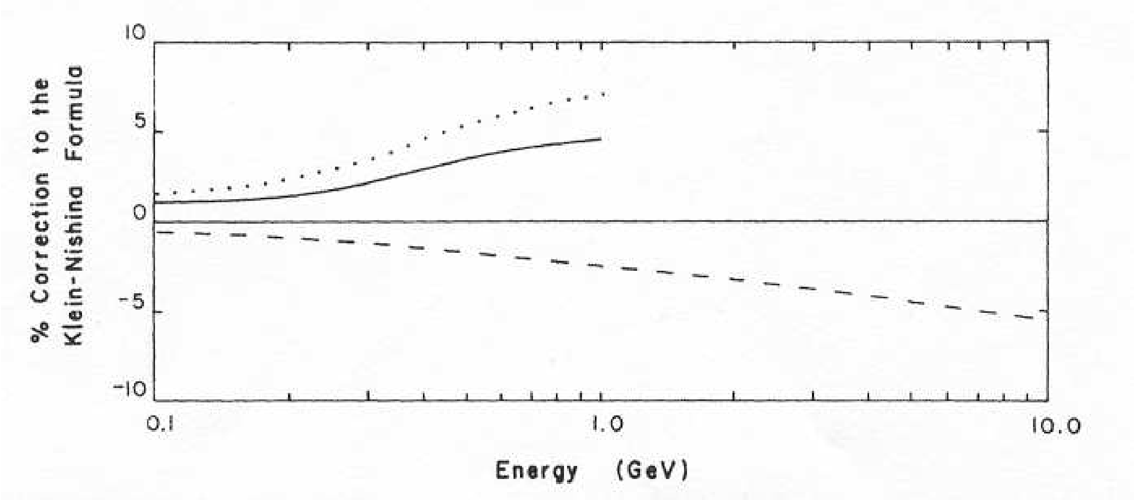

Figure 3: Radiative corrections (dashed curve), double-scattering contributions (dotted curve), and the total percentage correction (solid curve) to the Klein-Nishina formula (horizontal solid curve) [11].

1.2 Electron Compton Scattering

The Klein-Nishina formula for the differential cross section in the laboratory frame is given by [7]:

$$\frac{d\sigma}{d\Omega} = \frac{r_e^2}{2} \frac{1}{[1+\gamma(1-\cos\theta_\gamma)]^2} \left[1 + \cos^2\theta_\gamma + \frac{\gamma^2(1-\cos\theta_\gamma)^2}{1+\gamma(1-\cos\theta_\gamma)} \right], \tag{2}$$

where $\gamma = \frac{E_\gamma}{mc^2}$, θ_γ is the photon scattering angle, E_γ is the incident photon energy, m is the electron mass, and r_e is the classical electron radius. The total cross section is:

$$\sigma_c = 2\pi r_e^2 \left[\frac{1+\gamma}{\gamma^2} \left(\frac{2(1+\gamma)}{1+2\gamma} - \frac{1}{\gamma} \ln(1+2\gamma) \right) + \frac{1}{2\gamma} \ln(1+2\gamma) - \frac{1+3\gamma}{(1+2\gamma)^2} \right] \tag{3}$$

Two well-known features at high energies of the above cross sections are (a) the total cross section decreases approximately as $1/E_r$, and (b) $\frac{d\sigma}{d\Omega}$ for the scattered electron is sharply peaked at small angles. Measurement of the forward scattering photon and electron angles (θ_γ, θ_e) uniquely determine the incident photon energy E_r:

$$E_\gamma(\theta_\gamma, \theta_e) = mc^2(\cot\theta_e \cot\theta_\gamma - 1) \tag{4}$$

We plan to measure the absolute energy of the tagged photon at the $\sim 10^{-3}$ level by using this electron Compton scattering technique.

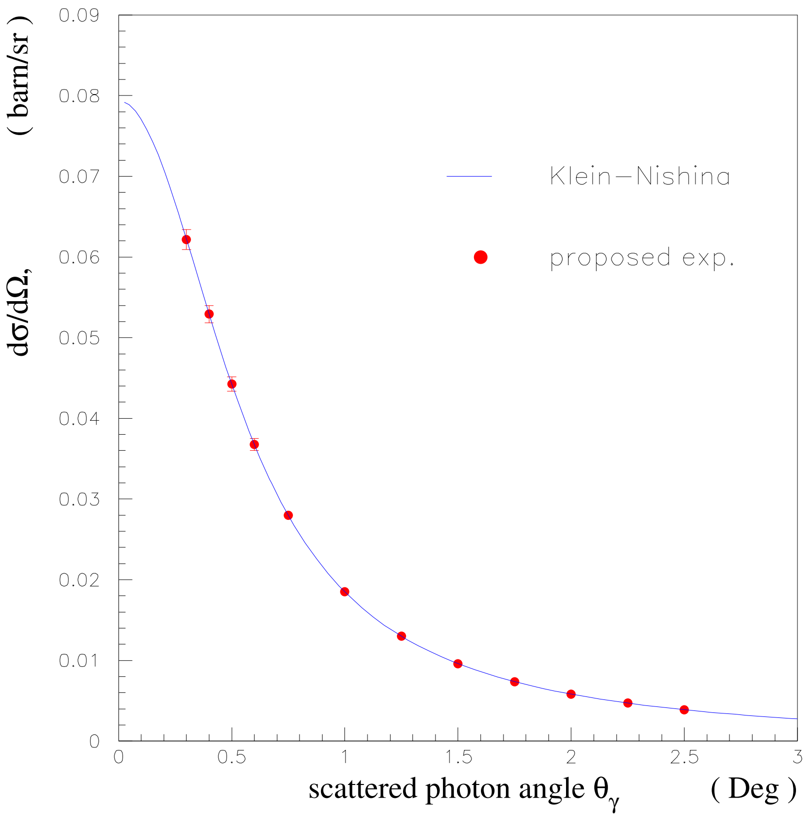

Figure 4: Electron Compton scattering differential cross sections for 5 GeV photon beam. The data points are the proposed experimental measurements projected on to the Klein-Nishina formula.

2 Experimental Setup

We propose to utilize the PrimEx experimental setup (figure 5) which includes: (1) the Hall B photon tagger; (2) a highly segmented hybrid electro-magnetic calorimeter (HYCAL) to detect both the scattered photons and the recoil electrons. (The pair-spectrometer shown in figure 5 will be off during the Compton measurement.) We also plan to use a 0.1% radiation length solid ^{9}Be target. A brief description of the experimental setup is given below (details can be found in [16]).

2.1 The Hall B Photon Tagger System

We propose to use a 6 GeV electron beam incident on a thin (10^{-4} radiation length) bremsstrahlung converter foil. The post-bremsstrahlung electrons will be momentum analyzed by the tagger magnet [17]. The focal plane detectors of the tagger cover a photon energy range from 20% to 95% of the incident electron energy (E_e). The detector system consists of two

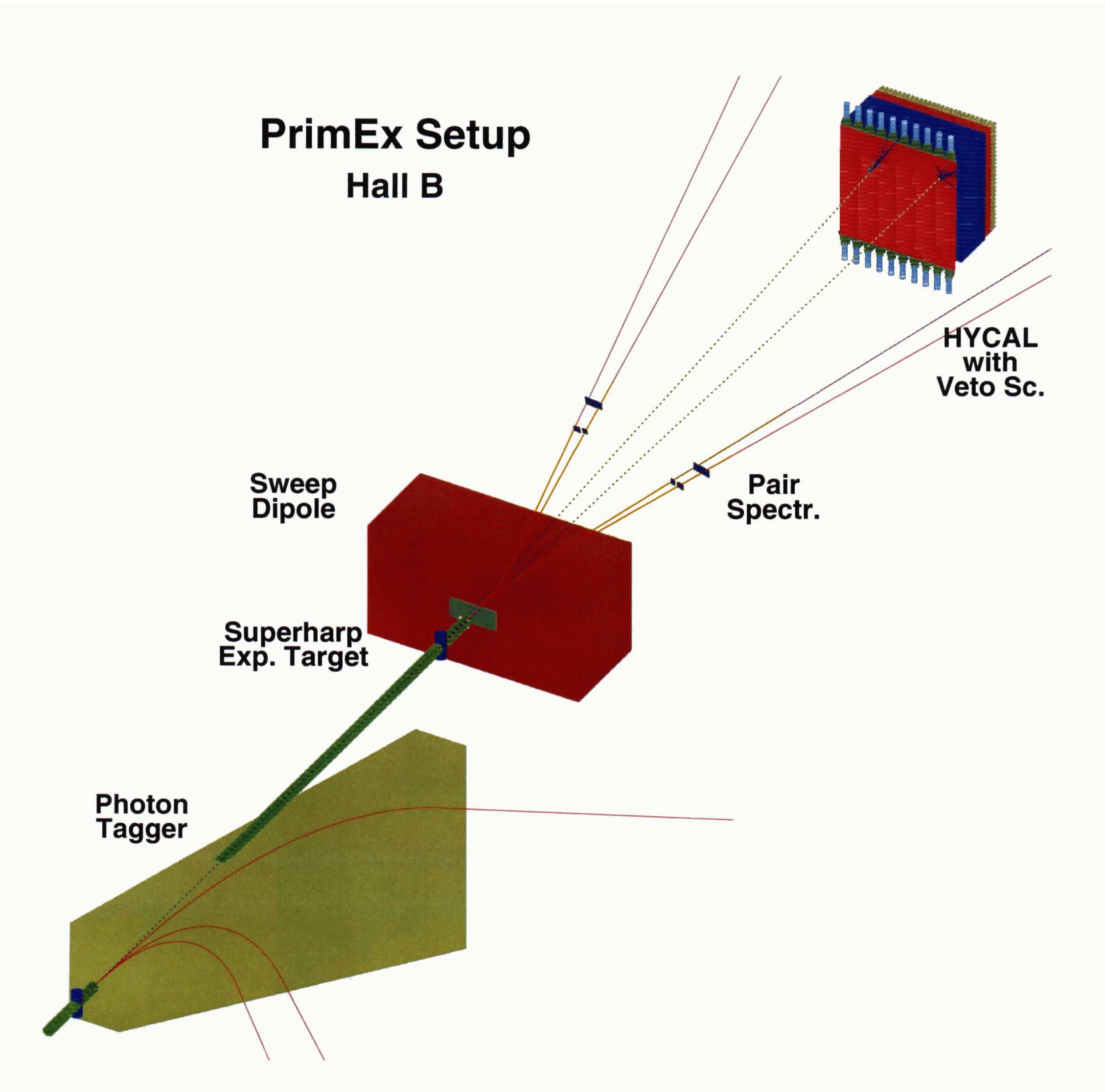

Figure 5: Experimental setup.

planes of counters: 384 overlapping scintillators which define 767 fine energy bins of width 0.001 E_e (the "E" counters), and 61 larger scintillators, each read out by two photo-multiplier tubes, and designed for good time resolution (the "T" counters). The sizes of the T-counters are designed to produce approximately equal counting rates in two groups. When all 61 T-counters are used, the total tagging rate can be as high as 50 MHz for the whole focal plane. A side view of the tagger system is shown in figure 6.

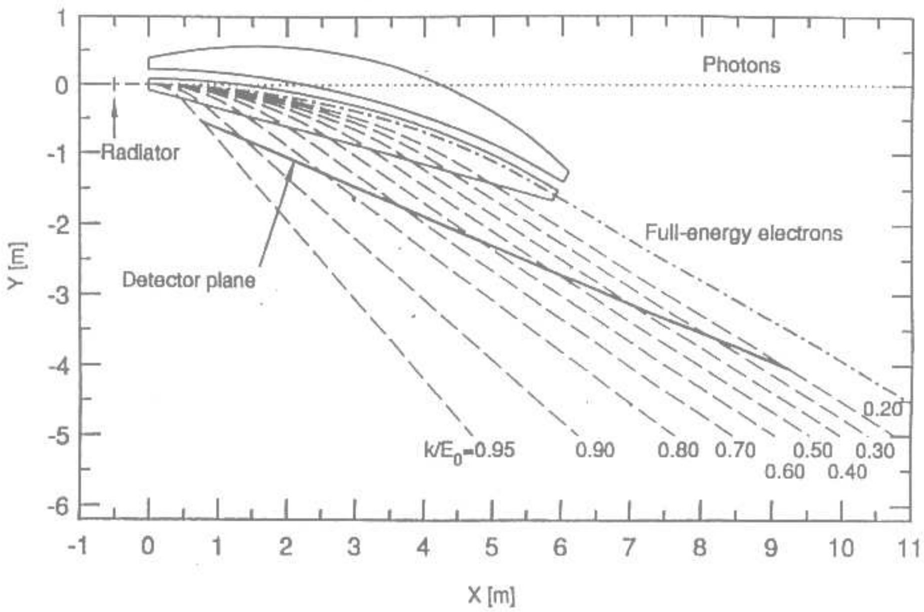

Figure 6: Side view of the Hall B photon tagging system. (Figure is from [17].)

2.2 Target

We plan to use a 0.1% radiation length ^{9}Be target. The target will be placed in the first collimator box behind the tagger to extend the distance from HYCAL in order to obtain higher angular resolution. The thickness of the target is determined by optimizing the effect of the multiple scattering in the target material and the counting rate. A relatively light target is chosen so that the initial electron atomic motion will have less effect on the photon beam energy determination. A more detailed discussion of multiple scattering and atomic electron motion effect is presented in section 4.

2.3 The Hybrid Calorimeter (HYCAL)

Both the scattered photons and the recoil electrons from Compton events will be detected in a highly segmented array of the Hybrid Shower Calorimeter (HYCAL). Currently, the PrimEx collaboration is constructing HYCAL (figure 7) for E99-014, an approved experiment in Hall

B to do a precision measurement of the π^0 lifetime. The detector array covers an area about 120×120 cm^2 transverse to the beam, with a 34×34 matrix of $2.05 \times 2.05 \times 18.00$ cm^3 $PbWO_4$ crystals in the center, and ~ 600 modules of $3.8\times3.8\times45$ cm^3 lead glass detectors in the outer region. We plan to reconstruct the incident photon beam energy from the scattering angles of the photons and electrons using only the central $PbWO_4$ crystal insertion of HYCAL in order to reach the highest possible angular resolution. On the other hand, the full acceptance of HYCAL will be used for the cross section analysis to cover a larger angular range. Based on beam test results on a crystal prototype detector carried out in 2001, the achieved energy and position resolutions were $\sigma_E/E \sim 1.3\%$ and $\sigma_x \sim 1.2$ mm, for a 4 GeV electron beam. The innermost and the outermost modules will be excluded from the fiducial volume of the detector in order to control and maintain coordinate resolution and high detection efficiency near the boundaries of the detector. Figure 8 shows the acceptance of Compton events for a 5 GeV photon beam by the central crystal part of the calorimeter as a function of the distance between the target and HYCAL. The HYCAL detector can be placed at about 9–12 meters downstream of the target for optimal acceptance efficiency and good angular resolution.

The Hybrid Calorimeter has been designed to provide high precision coordinate and energy information for the detected particles. In order to maintain this performance, periodic energy calibration runs will be carried out. In addition, an optical gain monitoring system will be used between successive calibration runs. This system will continuously monitor the gain of each detector channel and the data will be recorded for offline analysis. Combining both these techniques, we will reach gain stability at the level of 0.2%.

Charged particles will be identified by plastic scintillation counters in front of HYCAL.

3 Beam Energy Coverage and Kinematical Cuts

3.1 Beam Energy Coverage

With the experimental setup as described in section 2 and the HYCAL detector located at a distance of 12 m downstream of the target, we can simultaneously measure the photon beam energy in the 2.0–5.7 GeV range (figure 9).

3.2 Kinematical Cut for the Beam Energy Measurement

The opening angle ($\psi_{\gamma e} = \theta_\gamma + \theta_e$) between the recoil electrons and the scattered photons reaches a minimum in a special kinematical region where $\frac{\partial E_\gamma(\psi_{\gamma e},\theta_\gamma)}{\partial\theta_\gamma} = 0$. In this case, the determination of the incident photon energy is independent of the beam direction. To first order:

$$E_\gamma(\psi_{\gamma e}, \theta_\gamma + \Delta\alpha) = E_\gamma(\psi_{\gamma e}, \theta_\gamma) + \Delta\alpha \frac{\partial E_\gamma(\psi_{\gamma e}, \theta_\gamma)}{\partial\theta_\gamma} + \Theta(\Delta\alpha^2) \tag{5}$$

where $\Delta\alpha$ is the deviation of the beam from zero degrees.

When $\frac{\partial E_\gamma(\psi_{\gamma e},\theta_\gamma)}{\partial\theta_\gamma} = 0$, we have:

$$E_\gamma(\psi_{\gamma e}, \theta_\gamma + \Delta\alpha) = E_\gamma(\psi_{\gamma e}, \theta_\gamma) + \Theta(\Delta\alpha^2) \tag{6}$$

Figure 10 shows $\frac{\partial E_\gamma}{\partial \theta_{\gamma/e}}$ as a function of the photon and electron scattering angles. For a 5 GeV photon beam, when the electron and photon scattering angles approach 0.82^o, $\frac{\partial E_\gamma}{\partial \theta_e}$ and $\frac{\partial E_\gamma}{\partial \theta_\gamma}$ become zero, and the opening angle between the scattered photon and the recoil electron $\psi_{\gamma e}$ reaches the minimum. If one selects Compton events in the region near the minimum opening angle, the energy measurement is not sensitive to the systematic uncertainty of the beam direction. We propose to determine the absolute photon beam energy at the $\sim 0.1\%$ level by measuring the electron and photon scattering angles near the minimum opening angle.

Figure 11 shows the distribution of positions of the scattered photons and the recoil electrons in the $PbWO_4$ crystal part of HYCAL with different cuts. It is evident from these plots that the kinematical cuts on the scattered photon-electron opening angle will select mostly Compton events with symmetric pairs of electrons and photons.

4 Uncertainties in the Beam Energy Determination

Experimentally, we will measure the scattering angles of the electrons and the photons from Compton events and reconstruct the beam energy from the two-body kinematics. A Gaussian fit will be applied to the reconstructed photon beam energy distribution to obtain the mean $\bar{E}$, giving the absolute beam energy, and the σ. The statistical error on $\bar{E}$ will be given by $\sim \sigma/\sqrt{N}$, where N is the total number of Compton events in the distribution. In the following discussion, we assume 2×10^7 photons/s beam intensity over the full tagger acceptance on a 10^{-3} radiation length ^{9}Be target and 5 days of beam time.

4.1 Statistical Uncertainties

The main contributions to the statistical error in the absolute energy measurement of the photon beam are from: (1) the spatial resolution of the crystal detector; (2) multiple scattering; (3) beam spot size; and (4) the atomic motion effect of the struck electron. Detailed discussions on each item are given below.

4.1.1 Spatial Resolution of the Crystal Detector

Preliminary results from the beam tests in 2001 of the crystal prototype detector show that a spatial resolution (see figure 12) of $\sigma_x \sim 1.2$ mm was achieved with a 4 GeV electron beam. A scintillating fiber X-Y coordinate detector ($\sigma_x^{\rm fiber} \sim 0.6$ mm) was placed in front of the crystal detector during the test. No non-linearity is observed in the reconstructed position within experimental uncertainties. The σ_x varies with the location of the hit in the crystal face; it has the minimum value at the boundaries between two modules and is maximum at the center of each module. Based on these beam test results, Monte Carlo calculations were carried out for the spatial resolutions of the crystals using the following expressions:

$$\sigma_x = \frac{3.0}{\sqrt{E}} \cdot \left[1.0 + 0.2\sin(2.0\pi x/20.5 + \frac{3}{2}\pi)\right] \quad \text{(mm)} \tag{7}$$

$$\sigma_y = \frac{3.0}{\sqrt{E}} \cdot \left[1.0 + 0.2\sin(2.0\pi y/20.5 + \frac{3}{2}\pi)\right] \quad \text{(mm)} \tag{8}$$

where x and y are the position coordinates (in mm) of the particles hitting the front face of the crystals, and E is the particle energy (in GeV).

Figure 13 (a) shows the Monte Carlo calculation of the crystal calorimeter spatial resolution effect on the photon beam energy measurement. The σ_E of the measured beam energy distribution induced by the crystal detector resolution is about 70 MeV. Moreover, we are exploring the option to add a low-mass X-Y coordinate detector, for *e.g.*, a drift chamber in front of the HYCAL. It will enhance σ_E considerably, as shown in figure 14.

4.1.2 Multiple Scattering

A very important contribution to the statistical uncertainties is from the multiple scattering of electron in the target. In order to evaluate this effect, we assume that the deviation of the scattered electron from its initial direction can be approximated by a Gaussian distribution. Figure 13(b) shows that multiple scattering effects will increase the σ_E of measured beam energy distribution by about 20% compared to the no-scattering case shown in figure 13(a).

Figure 15 shows that the reconstructed beam energy resolution varies with the target thickness. A 10^{-3} radiation length of target is chosen for the proposed experiment based on this calculation.

4.1.3 Beam Spot Size

The photon beam spot size also adds to the overall statistical uncertainty in the absolute energy determination of the incident beam. Photons produced in the bremsstrahlung radiator by a 6 GeV electron beam will pass through the 6 cm pole gap of the tagger magnet and then through a 7.5 cm beam pipe. Thus, the photon beam is unobstructed out to an angle of about 70 m_e/E_e. Electron beam scans at the position of the radiator are carried out routinely in Hall B experiments, and these show no indications of a beam-halo. Based on GEANT simulation studies [16], the beam profile on the PrimEx target position, which is about 2 m downstream of the planned Compton target, for the high energy component of the beam, $E_\gamma > 5$ GeV, the expected beam spot is about 1.4 mm (FWHM). Therefore, we assume the beam profile at the Compton target are Gaussian in shape in both x and y directions with $\sigma_x = \sigma_y = 0.7$ mm. Results of beam spot size effects are shown in figure 13(c). Compared to a point-like beam spot, the σ_E of the reconstructed beam energy distribution increases about 3% due to finite beam-spot size effects.

4.1.4 Electron Atomic Motion Effect

In the previous discussion, we have assumed a photon interacting with a free electron in Compton scattering. However, for an atomic electron, Doppler broadening of the Compton

shell	A_{i1}	A_{i2}	ξ_{i1}	ξ_{i2}
K	0.9042	0.0958	3.4634	5.3326
L	0.9397	0.0603	0.5648	3.4130

Table 1: Momentum density distribution parameters for K- and L-shell atomic electrons for ^{9}Be.

spectrum will appear due to the atomic motion of the target electron. The electron atomic momentum-density distributions in the K and L shells can be described analytically by [19]:

$$I_i(p) = 4\pi p^2 \rho_i(p) = \frac{32}{\pi} \sum_{j=1}^{2} \frac{A_{ij}\xi_{ij}^5 p^2}{(\xi_{ij}^2 + p^2)^4}, \quad (i = K, L) \tag{9}$$

where $\rho_i(p)$ is the normalized momentum-density distribution, p is the momentum of the electron in atomic units, and A_{ij} and ξ_{ij} are parameters determined by requiring that the results should be equal to the corresponding Hartree-Fock results. The parameters for ^{9}Be are listed in table 1. Figure 16 shows the electron momentum density in ^{9}Be.

The resolution of the measured beam energy distribution becomes 12% larger when one considers the initial electron momentum in ^{9}Be atom, shown in figure 13(d), compared to Compton scattering off a free electron, shown in figure 13(c).

4.2 Systematic Uncertainties

The two major sources of systematic uncertainties contributing to the absolute value of the energy measurement are:

1. Uncertainty of the beam direction.
2. HYCAL misalignment.

In both cases they induce an uncertainty in the measured scattering angles of the electrons and the photons. As discussed earlier, applying a kinematical cut on the photon-electron opening angle will help to reduce the systematic errors.

There are two beam profile monitors in Hall B with about 50 m distance between them. Assuming a beam shift at the upstream beam monitor by about 1 mm, and a shift at the downstream monitor by about 3 mm, the maximum polar angle of the beam direction deviation could be:

$$\theta_0 = \frac{4}{50000} \sim 10^{-4} \text{ (rad)} \tag{10}$$

Considering the worst case, the initial photon beam deviates with a polar angle $\theta_0 = 10^{-4}$ rad and an azimuthal angle $\phi = 0.785$ rad, and HYCAL has a misalignment of $\Delta x = \Delta y = 1$ mm with respect to the incident beam. so that these two effects will enhance each other. Figures 17, 18 show Monte Carlo simulation studies of the systematic uncertainties in the measured beam energy for different incident photon beam energies including all statistical errors discussed earlier. For each step of 0.005 GeV initial beam energy shift (f igure 17), the reconstructed absolute beam energy gives correct answer within required errors. Our setup will simultaneously cover the 2.0–5.7 GeV energy region cross the photon tagger. The independent relative photon energy information from the tagger, will allow us cross check the systematic uncertainties. These studies indicate that combining all possible systematic and statistical errors, an uncertainty in the absolute beam energy determination of $\frac{\Delta E}{E} \sim 10^{-3}$ can be achieved.

5 Compton Scattering Cross Section Measurement

Parallel to the beam energy calibration measurements, the same data set will be used for obtaining the differential cross sections of Compton scattering by using the full acceptance of the HYCAL detector. As shown in figure 19, the Compton events in the region of photon scattering angles from 0.3^o up to 2.5^o can be detected by the HYCAL. The differential cross sections in the 2.0–5.7 GeV energy range will be measured with an estimated precision of $\sim$ 2% (figure4). The error bars shown in the figure are mainly dominated by the photon flux uncertainty.

Control of the photon flux at $\sim$ 2% accuracy is crucial for performing a precision measurement of the cross sections. Compton events are measured in coincidence with a tagged photon signal. The normalization of the cross section to the incident photon flux depends on knowing the number of tagged photons on target in each energy bin during the run. This number is not necessarily equal to the number of events recorded by the tagger counters because of two effects: (1) events in which a bremsstrahlung photon is produced but is absorbed before reaching the target, and (2) Møller scattering events in the bremsstrahlung radiator which produce an electron in the tagger counters without an accompanying photon. Events of the first type will be minimized by allowing the entire bremsstrahlung beam to travel in vacuum without collimation to the target. The second category of events is known to affect the tagging rate at the level of a few percent. The combination of these effects can be measured by removing the target and placing a lead glass total absorption counter (TAC) in the photon beam and recording the ratio of Tagger·TAC coincidences to tagger events. A detailed description of this technique is given in [16].

6 Experimental Considerations

6.1 Rate and Beam Time

For a 10^{-3} radiation length ^{9}Be target, the number of the electrons per cm^2 is:

$$\begin{aligned} N_{B_e} &= Z \cdot \frac{\rho t}{A} \cdot N_A \\ &= 4 \times \frac{1.848 \times 35.28 \times 10^{-3}}{9} \times 6.02 \times 10^{23} \\ &= 1.74 \times 10^{22} \end{aligned}$$

During the Compton run, the pair-spectrometer dipole in the beam-line will be turned off. We will not have a sweeping magnet to clean away the charged particle background from HYCAL as have been planned for the π^0 lifetime experiment. Therefore, we intend to use a lower beam intensity. On the other hand, a lower beam intensity will benefit the cross section measurements in order to maintain a stable photon flux. Using an incident beam intensity of $Q \sim 2 \times 10^7$ photons/s over the full acceptance of the tagger and an energy bin width of $\Delta E \sim E \times 10^{-3}$, the number of the photons in this bin is given by:

$$\begin{aligned} N_r &= Q \cdot \ln(E_h/E_l) \\ &\approx 2 \times 10^7 \times \ln(E_l(1+10^{-3})/E_l) \\ &\approx 2 \times 10^4 \qquad (\gamma/\text{second}) \end{aligned}$$

At 5 GeV, the total cross section for Compton scattering is 0.2647 mb. The expected Compton production rate for a 10^{-3} energy bin is:

$$\begin{aligned} R &= N_e \cdot N_r \cdot \sigma_t \cdot \varepsilon_{eff} \\ &\approx 1.74 \times 10^{22} \times 2 \times 10^4 \times 0.2647 \times 10^{-27} \times 0.18 \\ &\approx 1.66 \times 10^{-2} \qquad (\text{Hz}) \\ &\approx 1433 \qquad \text{events/day} \end{aligned}$$

We estimate to have 6 days of beam time to calibrate the absolute energy of tagged photon beam at $\sim 10^{-3}$ level in the 2.0–5.7 GeV energy range. In parallel, we will measure the differential cross sections of Compton scattering in the forward angles.

6.2 Background

The scattered photons and the electrons will be detected in coincidence, and Compton events will be selected based on two main criteria:

- the coplanarity of the photon and electron;
- the angular and energy correlation according to the two-body kinematics.

As we are proposing to run with the photon luminosity lower by about two orders of magnitude compared to the π^0 lifetime experiment, we expect that the total background rate will be considerably lower than for that experiment. The two major processes, photon pair-production and triplet-production of electrons, have competing cross sections compared to the Compton scattering process. For the high energy incident photon beam, however, the pair-production is mostly limited to the forward direction, and passes through the central opening in HYCAL. The triplet-production process has a much lower cross section and will dominate the accidental count rate. We also expect backgrounds from Compton events produced in material other than target. Figure 20 shows the correlations of scattered photon angle and energy for Compton events produced on the target and other materials 4 m downstream of the target. It clearly indicates that we are able to distinguish these different Compton events kinematically.

7 Summary

We propose to calibrate the absolute energy of the tagged photon beam in Hall B at the level of 10^{-3} via the electron Compton scattering process near the minimum opening angle of the scattered photon-electron pair. With a single experimental setting, we will simultaneously cover the 2.0–5.7 GeV energy region. This measurement will reduce the current uncertainty ($\sim$1%) of the tagged photon beam energy calibration by an order of magnitude. The same data set will also allow us to extract the differential cross sections in the forward region, scattered photon angles (0.3^o–2.5^o), for Compton scattering with an estimated precision of about $\sim$2%. This experiment would be the first precision measurement on this fundamental QED process in the few GeV energy range, and will shed light on the higher order corrections to the Klein-Nishina formula.

We are requesting 6 days of beam time at 6 GeV. The major equipment for this experiment includes the Hall B photon tagger and the PrimEx HYCAL calorimeter.

References

[1] A. H. Compton, Bull. Natl. Res. Counc. (U.S) 20, 19 (1922); *Phys. Rev.*, **21**, 483 (1923).

[2] I.M. Brown and R.P. Feynaman, *Phys. Rev.*, **85**, 231(1952).

[3] Till B. Anders, *Nucl. Phys.*, **87**, 721 (1967).

[4] K.J. Mork, *Phys. Rev.*, **A4**, 917 (1971).

[5] G. Bellettini et al., *Il Nuova Cimento*, **66**, no. 1, 243 (1970).

[6] A. Browman et al., *Phys. Rev. Lett.*, **33**, 1400 (1974).

[7] O. Klein and Y. Nishina, *Z. Phys.*, **52**, 853 (1929).

[8] I. Tamm, *Z. Phys.*, **62**, 545 (1930).

[9] F. Mfandl and T.H.R. Skyrme, *Proc. R. Soc. London*, **A215**, 497 (1952).

[10] M. Ram and P.Y. Wang, *Phys. Rev. Lett.*, **26**, 476 (1971); *ibid.* **26**, 1210(E) (1971).

[11] A.T. Goshaw et. al.,*Phys. Rev.*, **D18**, 1351 (1978).

[12] F. H. Coensgen, University of California Radiation Laboratory Report UCRL-2413, 1953 (unpublished).

[13] L. V. Kurnosova et al., *Zh. Eksp. Theor. Fiz.*, **30**, 690 (1956) [Sov. Phys. - JETP 3, 546 (1956)].

[14] J. D. Anderson et. al., *Phys. Rev.*, **102**, 1626 (1956).

[15] B. Gittelman et. al., *Phys. Rev.*, **171**, 1388 (1968).

[16] TJNAF PAC 15 proposal *E99-014*; *PrimEx Conceptual Design Report for NSF MRI grant in 2000.*

[17] D.I. Sober, *A Guide to the Optics of the Tagged Photon Magnet*, CLAS Note 91-012.

[18] K. Mengel, R. Novotny, R. Beck, *et al.*, *IEEE Trans. Nucl. Sci.*, **45**, 681-685 (1998).

[19] Y.F. Chen, C.M. Kwei and C.J. Tung, *Phys. Rev.*, **A47**, 4502 (1993).

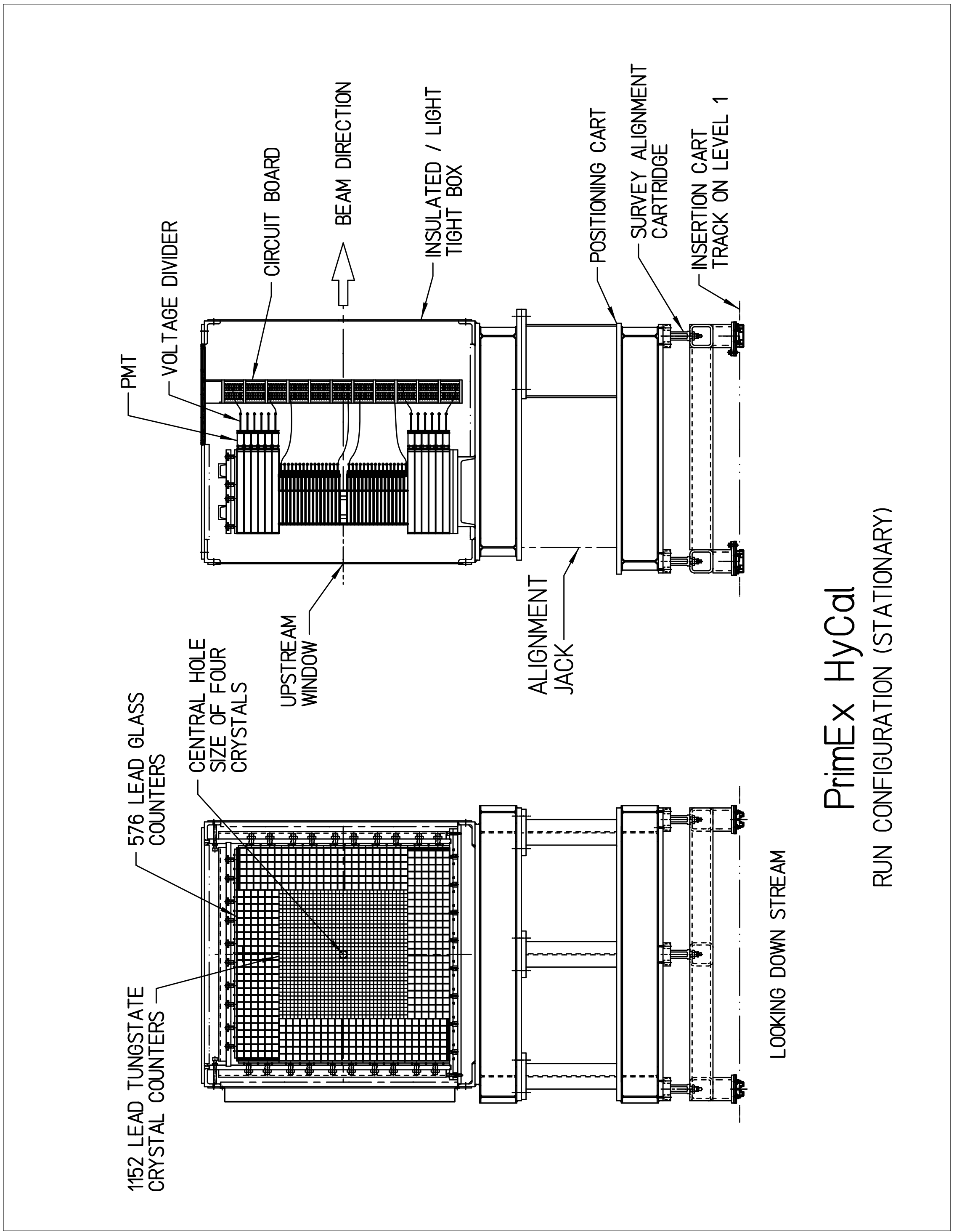

Figure 7: Schematic view of the HYCAL electro-magnetic calorimeter with the transporter.

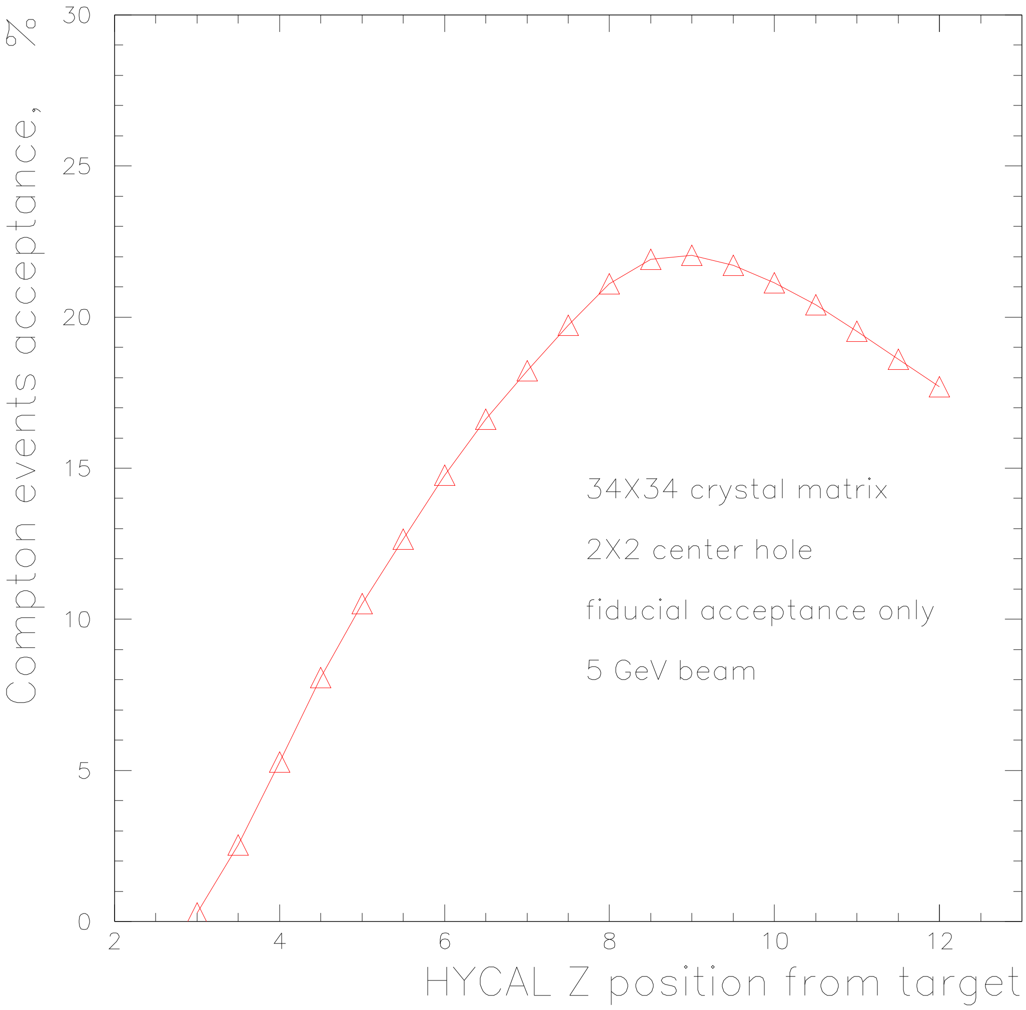

Figure 8: $PbWO_4$ crystal array acceptance efficiency for Compton events vs. the distance between the target and HYCAL.

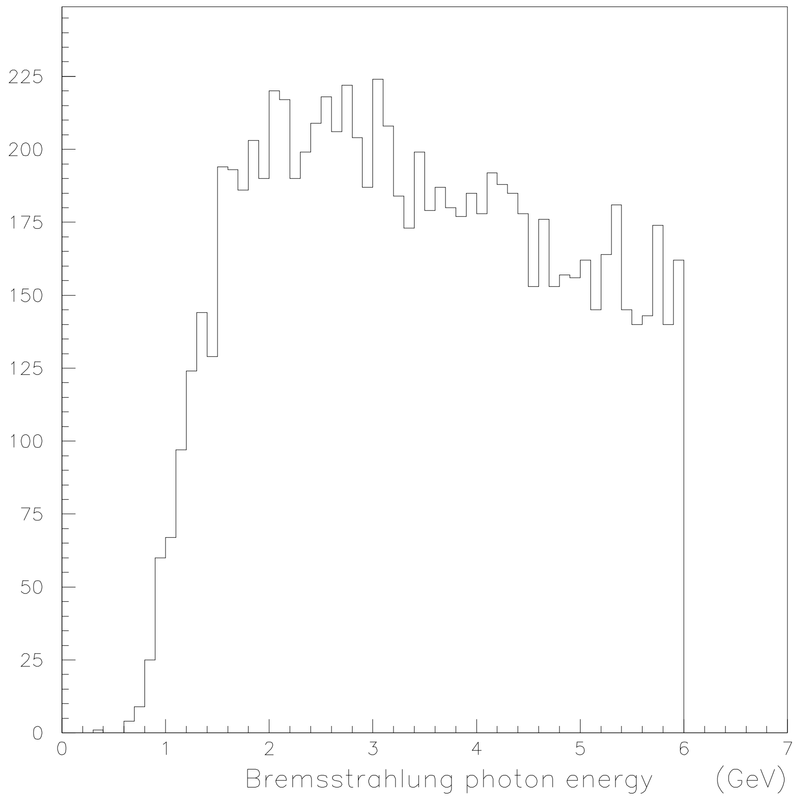

Figure 9: GEANT simulations of the distribution of the bremsstrahlung photon beam energy covered by the experimental setup with HYCAL at 12 m downstream of the target.

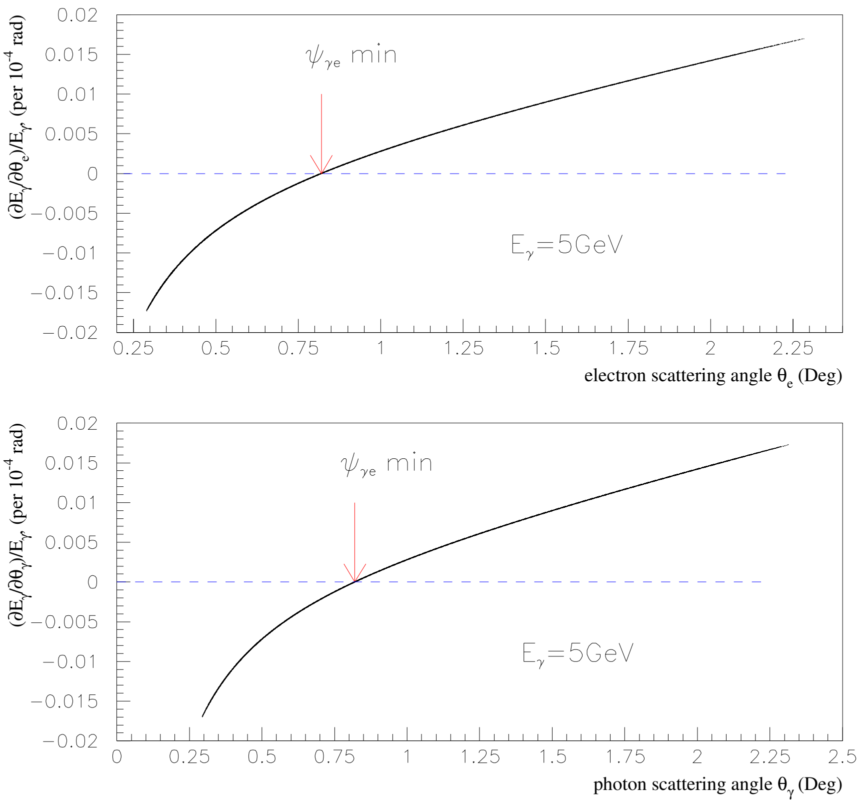

Figure 10: The $\frac{\partial E_\gamma}{\partial \theta_{\gamma/e}}$ as a function of electron and photon scattering angles.

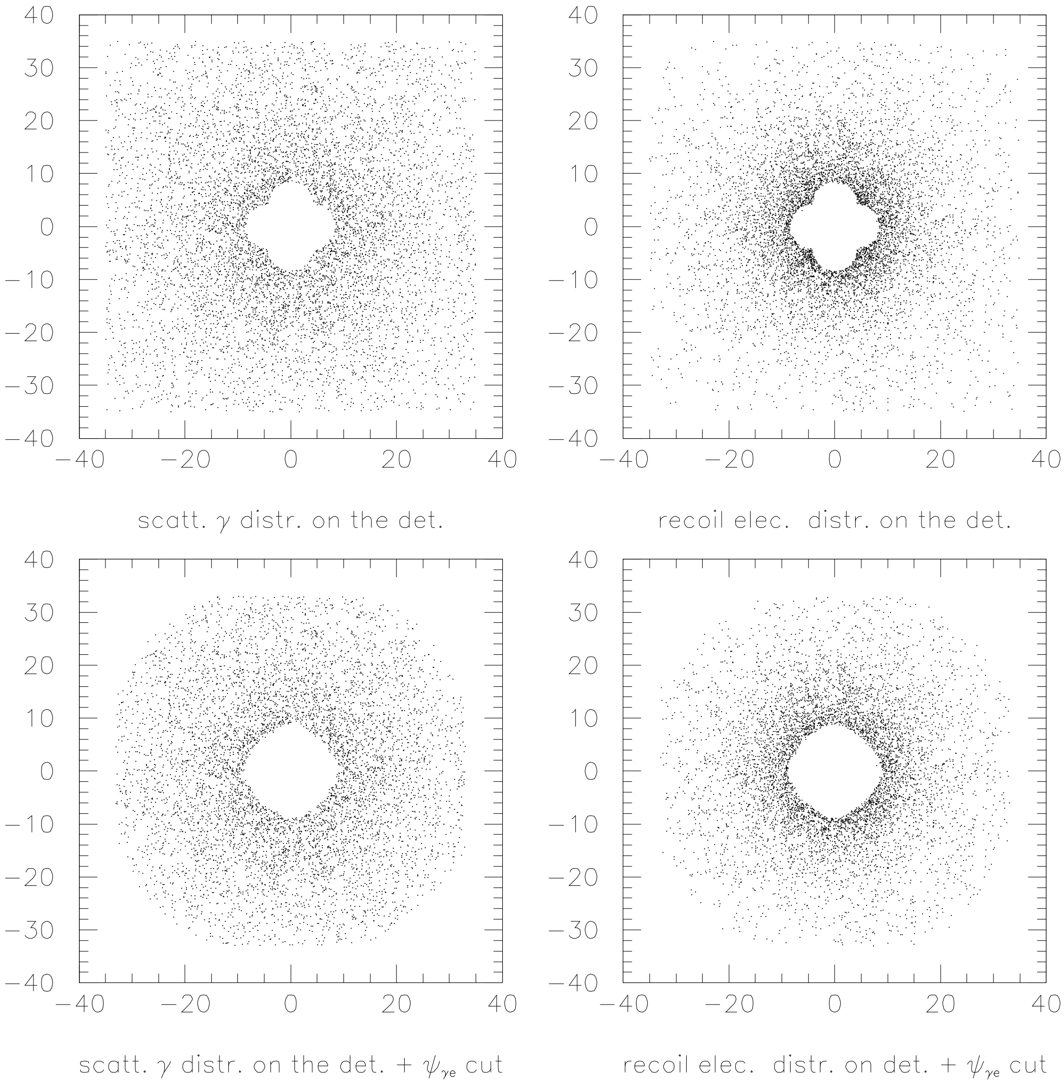

Figure 11: GEANT simulations of the distributions of scattered photons and recoil electrons in the $PbWO_4$ detector. (a) and (b) are without the kinematical cuts, (c) and (d) are with the cut on the photon-electron opening angle $\psi_{\gamma e} < 2.1^o$. (HYCAL is 12 m downstream of the target.)

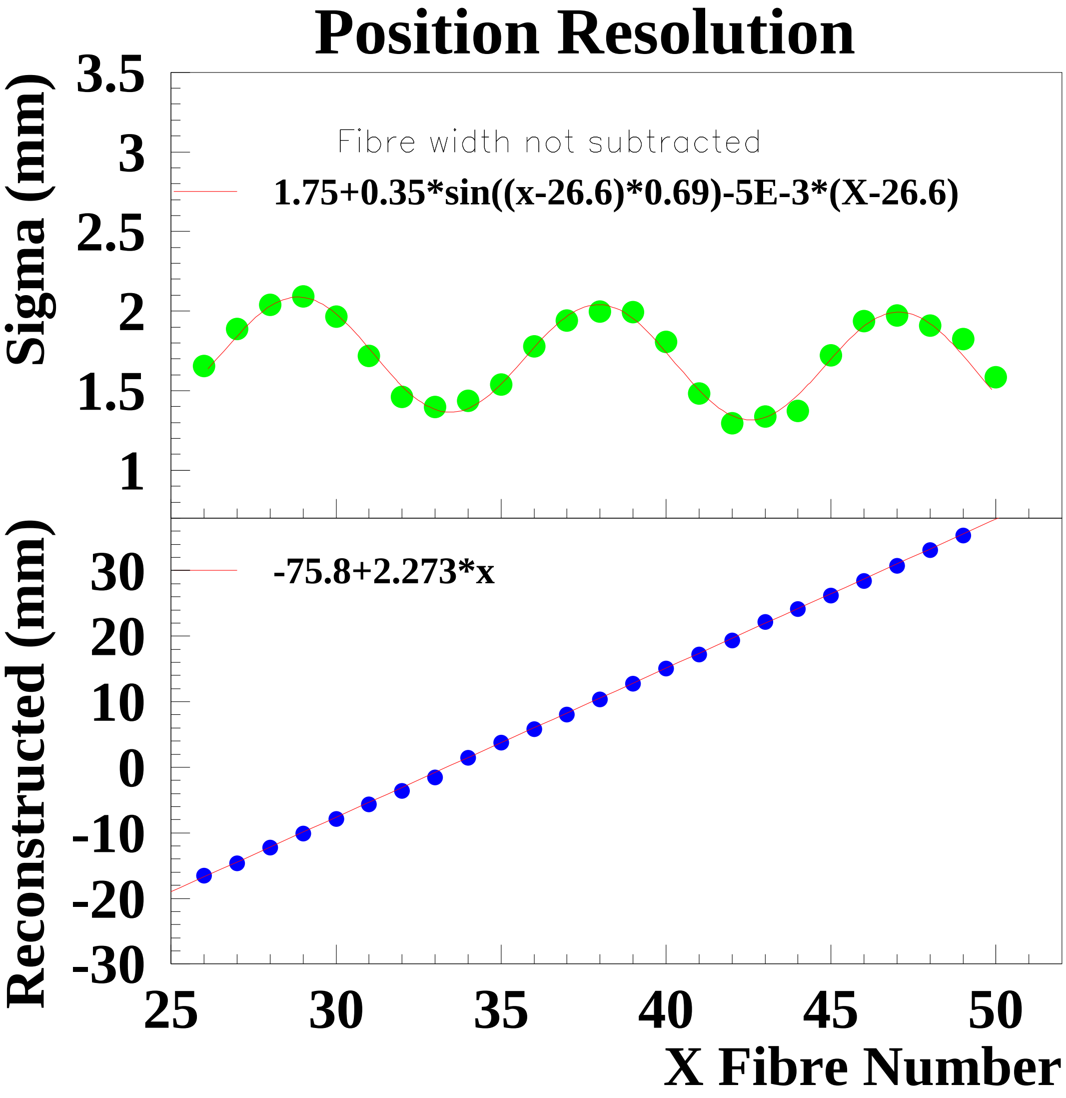

Figure 12: Position resolution (*top panel*) and reconstructed position (*bottom panel*) of $PbWO_4$ crystal detector *versus* X-fiber number of X-Y coordinate detector.

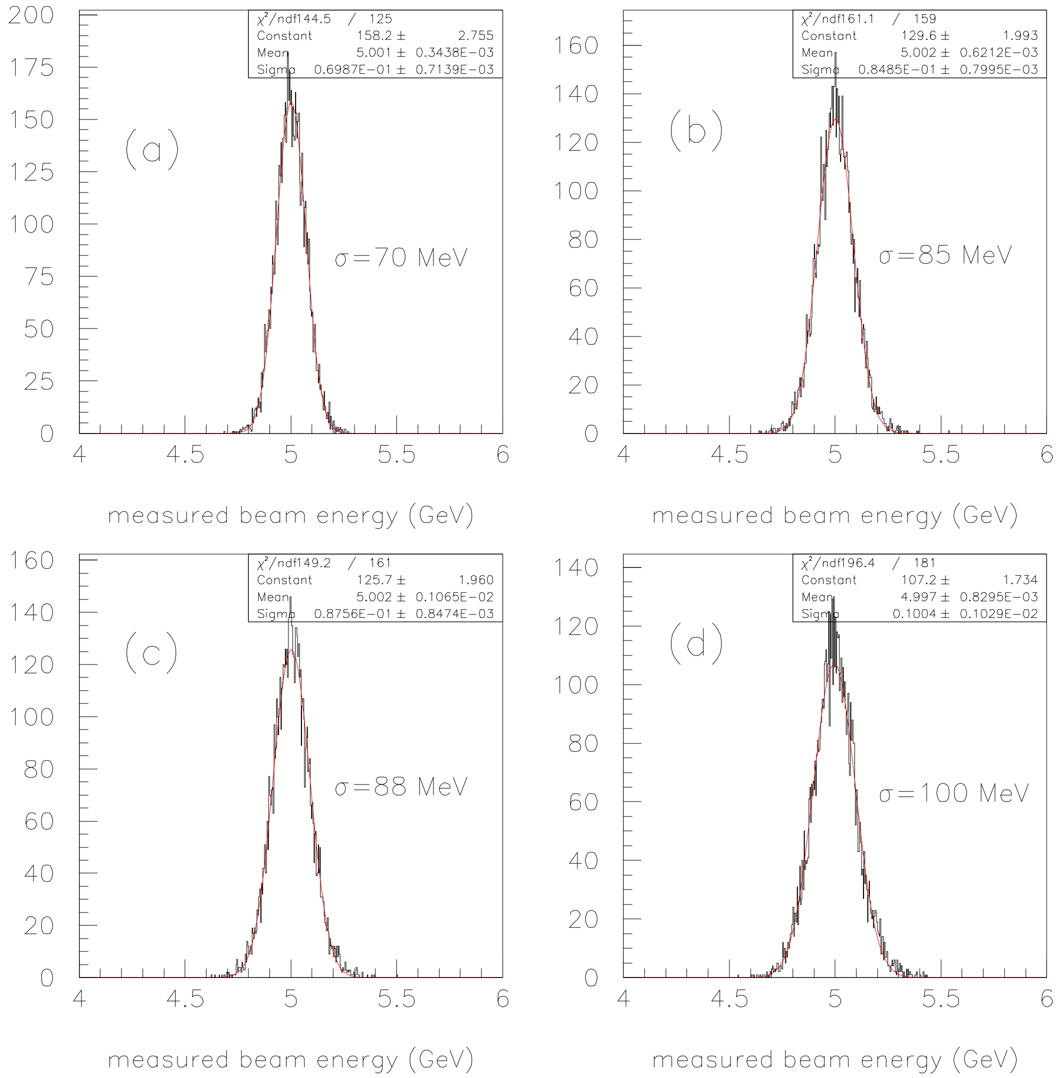

Figure 13: GEANT simulation of the single event errors in the absolute energy measurement of the beam. (a) Only the spatial resolution σ_x of the crystals is considered; (b) multiple scattering in target in addition to (a); (c) beam spot size on the target ($\sigma_x^{\mathrm{beam}} = \sigma_y^{\mathrm{beam}} = 0.7$ mm) in addition to (b); (d) atomic motion effect of the struck electron in ^{9}Be in addition to (c).

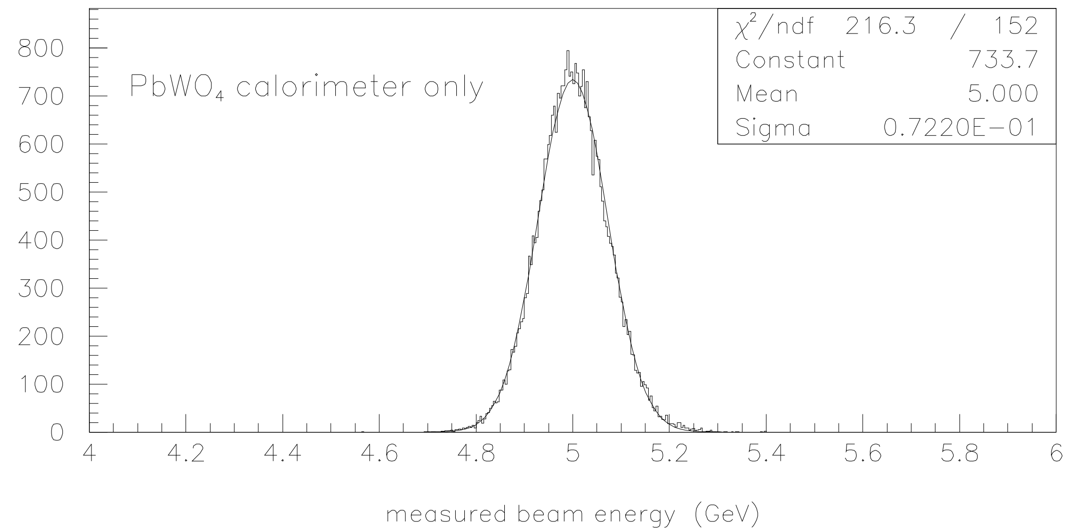

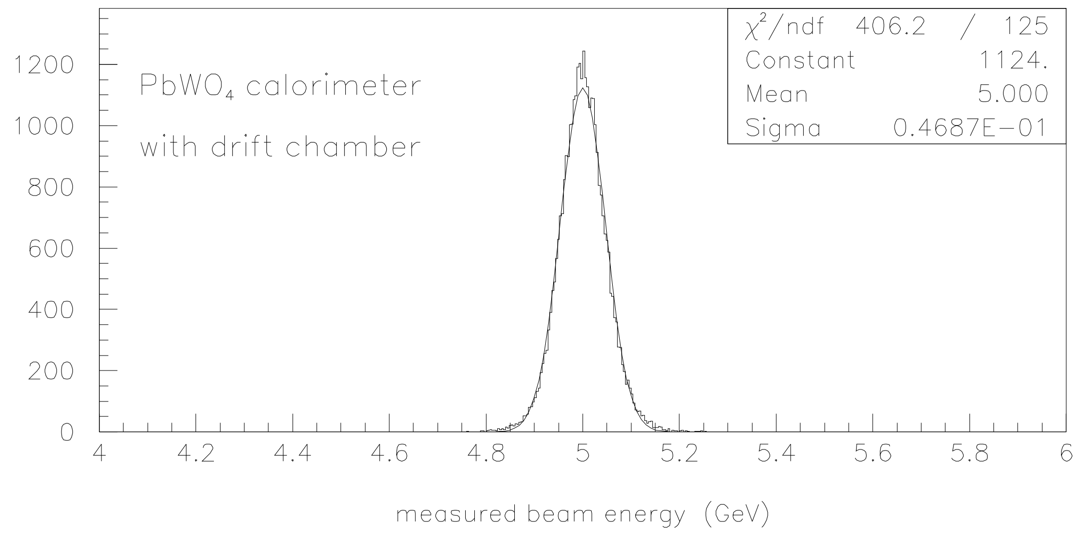

Figure 14: Monte Carlo simulation of $PbWO_4$ crystal detector for measured beam energy resolution at $E_\gamma = 5$ GeV with and without a drift chamber in front of the detector.

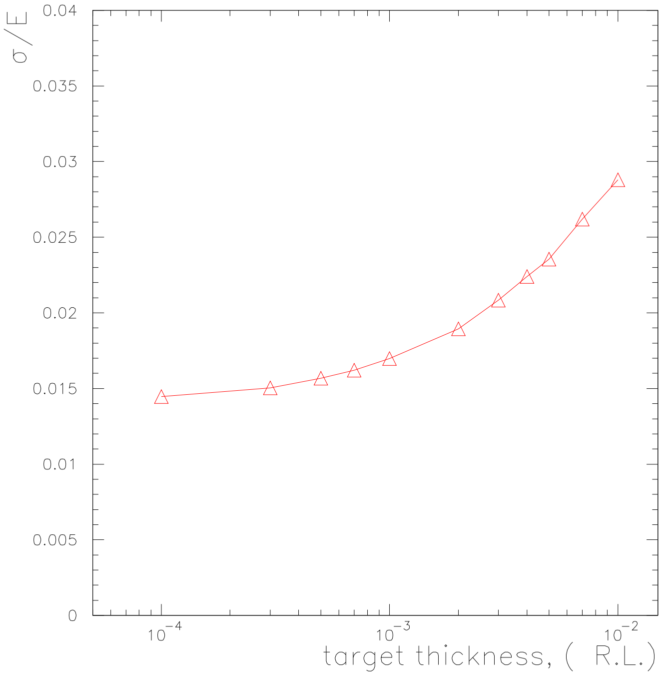

Figure 15: Simulation of the reconstructed photon energy resolution vs. target thickness including the spatial resolution of the crystal detector.

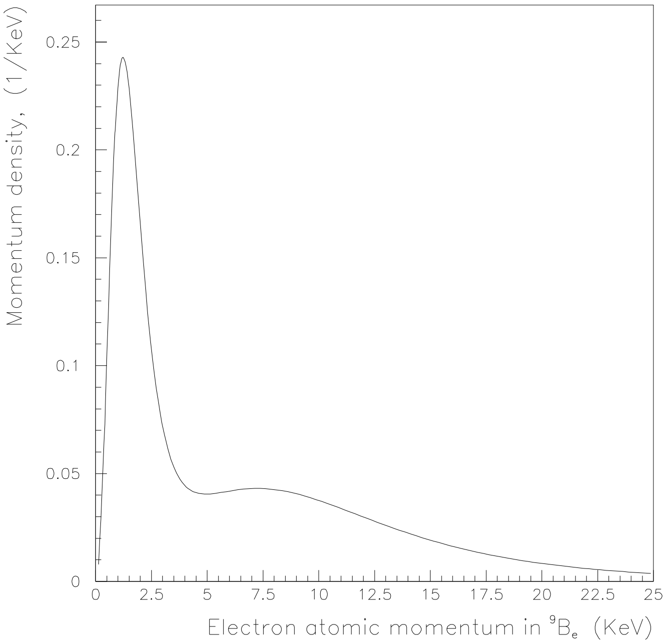

Figure 16: Momentum density distribution for atomic electrons in ^{9}Be.

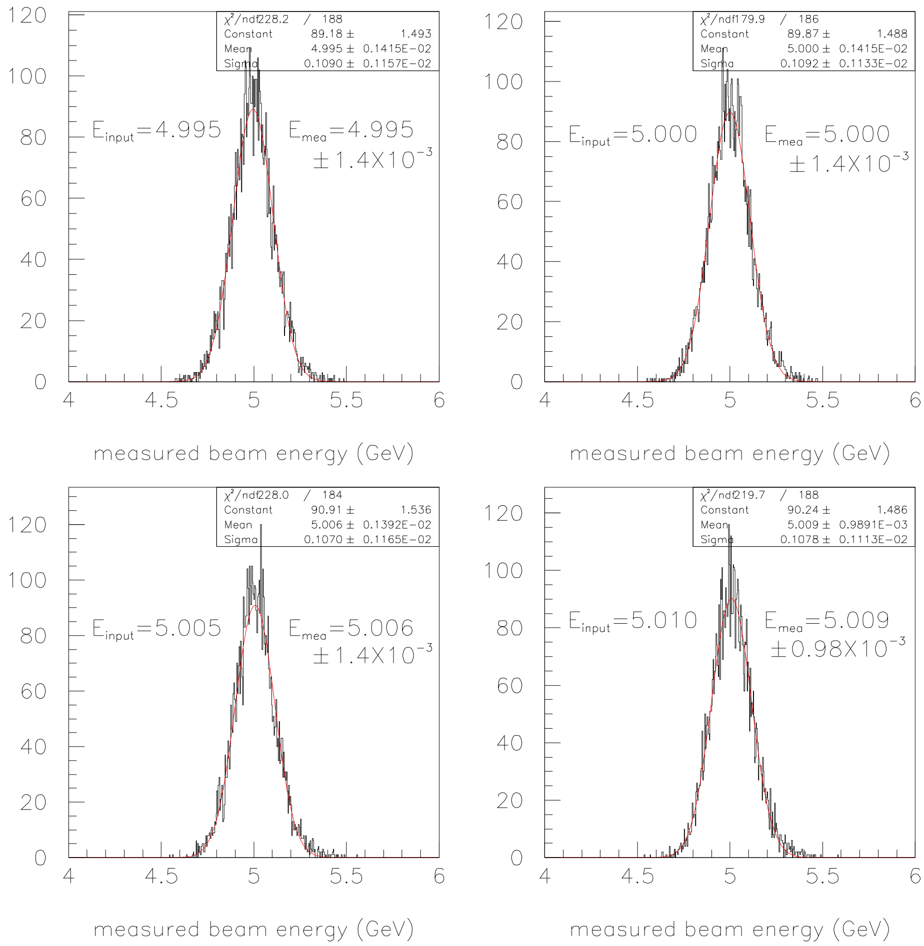

Figure 17: Monte Carlo simulation of measured beam energy distribution for four different initial beam energies, 4.995, 5.000, 5.005 and 5.010 GeV. A kinematical cut $\psi_{\gamma e} < 2.1^o$ is applied in all cases.

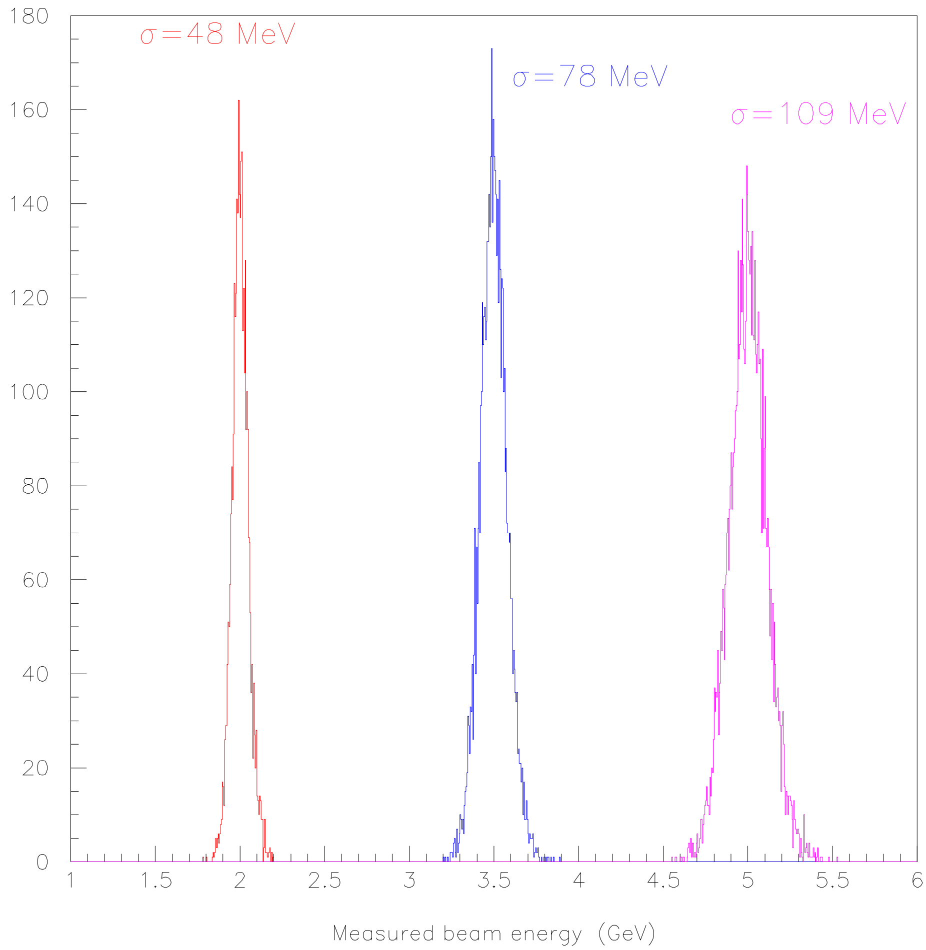

Figure 18: Monte Carlo simulation of measured beam energy distribution for three different initial beam energies, 2.000, 3.500, and 5.000 GeV.

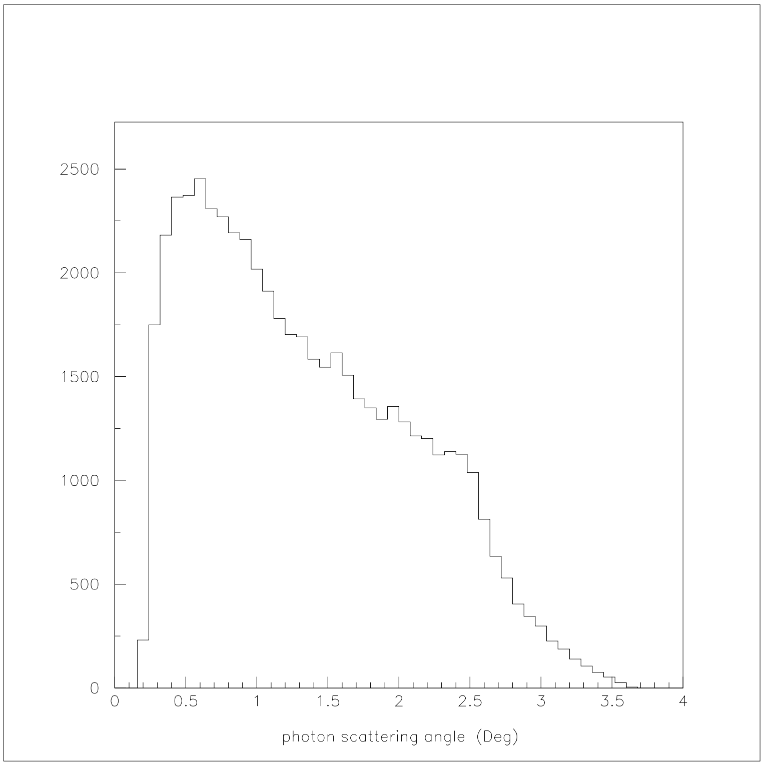

Figure 19: Simulations of angular acceptance of HYCAL at a distance of 12 m between the target and the detector.

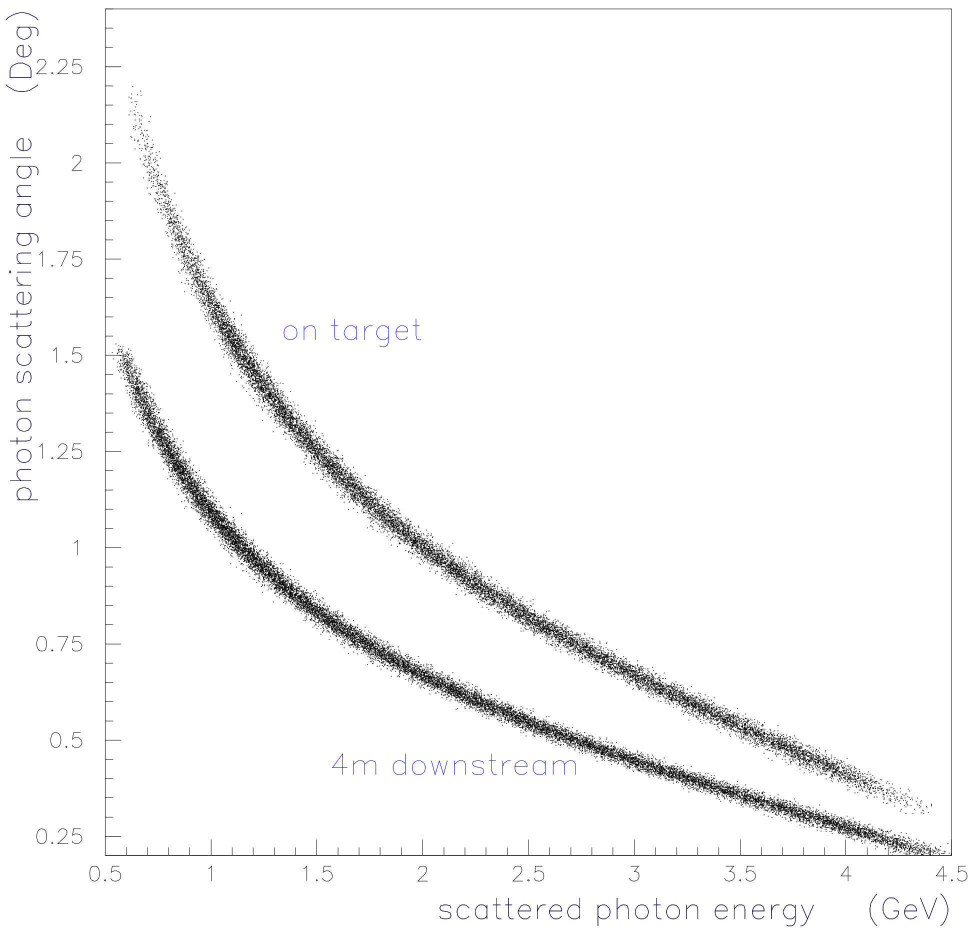

Figure 20: Monte Carlo simulations of Compton events produced at different Z positions along the incident beam direction.